Available online at www.sciencedirect.com
ScienceDirect
Journal of Sound and Vibration 307 (2007) 52–68
JOURNAL OF SOUND AND VIBRATION
www.elsevier.com/locate/jsvi

Wavelet-based outlier analysis for guided wave structural monitoring: Application to multi-wire strands

Piervincenzo Rizzo[a], Elisa Sorrivi[b,c], Francesco Lanza di Scalea[b,*], Erasmo Viola[c]

[a]*Department of Civil & Environmental Engineering, University of Pittsburgh, 949 Benedum Hall, 3700 O'Hara Street, Pittsburgh, PA 15360, USA*

[b]*NDE & Structural Health Monitoring Laboratory, Department of Structural Engineering, University of California, San Diego, 9500 Gilman Drive, M.C. 0085, La Jolla, CA 92093-0085, USA*

[c]*Dipartimento di Ingegneria delle Strutture, dei Trasporti, delle Acque, del Rilevamento, del Territorio (DISTART), Universita' degli Studi di Bologna, Via Risorgimento 2, 40136 Bologna, Italia*

Received 3 August 2005; received in revised form 18 September 2006; accepted 14 June 2007

Abstract

In this paper we describe a method based on outlier analysis and the wavelet transform for structural damage detection based on guided ultrasonic waves. The basic idea is to de-noise and compress the ultrasonic signals by the discrete wavelet transform and use the relevant wavelet coefficients to construct a unidimensional or multidimensional damage index. The damage index is then fed to an outlier analysis to detect anomalies that are representative of structural defects. By extracting the essential information from the ultrasonic signals, the dimension of the damage index is kept at a minimum, as desirable for continuous structural monitoring. The general framework is applied to the detection of notch-like defects in a seven-wire strand by using built-in magnetostrictive devices for ultrasound transduction. Random noise is digitally added to the raw ultrasonic measurements to create statistical populations of the baseline (undamaged) conditions and the damaged conditions. This application demonstrates the effectiveness of the multidimensional analysis compared to the unidimensional analysis, while keeping the number of features as low as four.

1. Introduction

The progressive aging of engineering systems increases the demand for structural monitoring, which includes damage detection and sizing. The development of an effective and robust monitoring strategy can prevent fatalities and reduce maintenance/repair costs. In recent years statistical approaches have gained increased attention for structural damage detection; generally, these methods are based on the evaluation of certain damage-sensitive features that are measured on the structure of interest. One such statistical approach is based on outlier analysis which is a novelty detection method that establishes whether a new configuration of the system is discordant or inconsistent from the baseline configuration which consists of an existing set of data (or patterns) that describe the normal operative conditions. The novelty detection

*Corresponding author. Tel.: +1 858 822 1458; fax: +1 858 534 6373.
E-mail address: flanza@ucsd.edu (F. Lanza di Scalea).

0022-460X/$ - see front matter © 2007 Elsevier Ltd. All rights reserved.
doi:10.1016/j.jsv.2007.06.058

approach belongs to the unsupervised learning class of pattern recognition. As such, it offers the fundamental advantage that information on the damage conditions do not need to be known a priori, contrarily to the supervised learning class. The unsupervised learning approach is particularly useful when it is difficult to simulate damage prior to the deployment and use of the monitoring system, as in the case of many structures in service.

The framework of outlier analysis is available in classical statistical textbooks [1]. The application of the method to diagnose structural damage was first presented by Worden [2]. In this work the reduced stiffness of a simulated lumped-mass system was detected by using the dynamic transmissibility function as the damage-sensitive feature. A 50-dimensional feature vector was constructed by discretizing the transmissibility function into 50 points. The approach was later extended by Worden et al. [3] to the detection of three different damage states, simulated by reducing the stiffness between two masses by 1%, 10% and 50% of the original, pristine value. The 50-point transmissibility function between the two masses was, again, considered as the damage-sensitive feature vector. Fifty-dimensional feature vectors were also considered in novelty detection for the structural monitoring of composite plates [4] and wings of a Gnat aircraft [5]. The feature vectors in these work consisted of discretized ultrasonic Lamb waves and transmissibilities along the stringers, respectively. Another application was the defect detection in running rotors [6].

The object of the present study is to apply novelty detection to guided ultrasonic waves analyzed by the discrete wavelet transform as a basis to construct the damage-sensitive features. The use of features extracted from the discrete wavelet transform analysis for novelty detection is not entirely new. At least one recent work [7] used the discrete wavelet transform coefficients of strain time series to formulate a vector dynamic regression model for the identification of outlier events in a bridge. The purpose of the discrete wavelet transform in the present work is to de-noise and compress guided ultrasonic wave measurements taken from structural components with finite cross-sectional dimensions, as opposed to vibration measurements representative of the global behavior of the structure. The de-noising and compression abilities of the discrete wavelet transform applied to ultrasonic measurements are well documented [8–14]. The effectiveness of the discrete wavelet transform applied to guided ultrasonic wave testing for defect detection and classification based on supervised learning has been demonstrated in steel strands [15,16], pipes [17] and railroad tracks [18]. This paper extends these previous works by incorporating the novelty detection as the unsupervised learning method of damage detection and sizing. The method is applied to the structural monitoring of seven-wire strands used in prestressed concrete structures and cable-stayed or suspension bridges. The paper presents first a basic review of univariate and multivariate outlier analysis, followed by the essential theory of the discrete wavelet transform and then the application to damage detection in strands.

2. Outlier analysis

An outlier is a datum that appears inconsistent with a set of data, the baseline, that describes the normal condition of the structure under investigation. Ideally, if outlier analysis is used for detecting damaged states, the baseline should include normal variations in environmental or operative conditions of the structure (e.g. temperature, humidity, loads) [19]. However, it is generally difficult to account for all of the environmental variables that may affect a damage-sensitive set of features. In this study different levels of random noise were digitally added to the guided ultrasonic wave measurements in order to represent possible variations in signal-to-noise ratio of the measurements, the most critical parameter affecting the damage-sensitive features considered in this study. Variations in ultrasonic signal-to-noise ratio can be originated, in practice, by a number of factors including changing electrical power to the ultrasonic transmitter, changing sensor/structure ultrasonic transduction efficiency, changing environmental temperature affecting ultrasonic attenuation losses and changing prestressing levels also affecting attenuation in multi-wire strands [14].

2.1. Outliers in univariate data

In the analysis of one-dimensional elements, the detection of outliers is a straightforward process based on the determination of the discordancy between the one-dimensional datum and the baseline. One of the most

common discordancy tests is based on the deviation statistics, z_ζ, defined as

$$z_\zeta = \frac{|x_\zeta - \bar{x}|}{\sigma}, \tag{1}$$

where x_ζ is the potential outlier, and $\bar{x}$ and σ are the mean and the standard deviation of the baseline, respectively. The mean and the standard deviation can be calculated with or without the potential outlier depending upon whether inclusive or exclusive measures are preferred. The value of z_ζ is then compared to a threshold value, discussed later, in order to determine whether the datum x_ζ is an outlier (above the threshold) or not. By simple algebra manipulations, Eq. (1) can be rewritten as

$$z_\zeta = \left|\frac{x_\zeta}{\sigma} - \frac{\bar{x}}{\sigma}\right| = |mx_\zeta + q|, \tag{2}$$

where

$$\begin{cases} m = \frac{1}{\sigma}, \\ q = -\frac{\bar{x}}{\sigma}. \end{cases} \tag{3}$$

The deviation statistics thus belongs to a straight line whose slope, m, is inversely proportional to the standard derivation of the baseline. The parameter m can be viewed as the sensitivity of the damage detection procedure that increases with decreasing variability of the baseline conditions.

2.2. Outliers in multivariate data

A set of p-dimensional (multivariate) data consists of n observations in p variables. The discordancy test equivalent to Eq. (1) is expressed by the Mahalanobis squared distance, D_ζ, which is a non-negative scalar defined as

$$D_\zeta = (\{x_\zeta\} - \{\bar{x}\})^{\mathrm{T}}[K]^{-1}(\{x_\zeta\} - \{\bar{x}\}), \tag{4}$$

where $\{x_\zeta\}$ is the potential outlier vector, $\{\bar{x}\}$ the mean vector of the baseline, $[K]$ the covariance matrix of the baseline and T represents a transpose matrix.

As in the univariate case, the baseline mean vector and covariance matrix can be inclusive or exclusive. In the present study, since the potential outliers are always known a priori, both z_ζ and D_ζ are calculated exclusively without contaminating the statistics of the baseline data.

2.3. Computation of the threshold

In order to determine whether a new datum (uni- or multidimensional) is an outlier, the corresponding value of z_ζ or D_ζ has to be compared to a threshold. When the available number of baseline data is limited, it is common practice to compute the threshold based on a Monte Carlo simulation generating a large number of random data to properly represent the baseline statistical distribution [3,6,20]. In the present study the baseline data set consisted of a large number of samples (300) that was generated by corrupting the ultrasonic measurements with digital random noise. It was found that this number of samples sufficiently represented the statistical distribution as a Gaussian curve, thus a Monte Carlo simulation was not required. Once the values of z_ζ and D_ζ of the baseline distribution were determined, the threshold value was taken as the usual upper value of 3σ, equal to 99.73% of the Gaussian confidence limit. Thus if a new datum was classified as an outlier, theoretically there was only a 0.27% chance of a "false positive" reading.

3. The discrete wavelet transform analysis

Since the main novelty of the present work is the use of discrete wavelet transform representations of guided ultrasonic wave signals as input data for the outlier analysis, a brief overview of this signal processing is given.

The wavelet decomposition of a function $f(t)$ is calculated from the following inner product:

$$W_{j,n} = \int_{-\infty}^{+\infty} f(t)\psi_{j,n}(t)^* \mathrm{d}t, \tag{5}$$

where $\psi_{j,n}(t)^*$ is the conjugate of the mother wavelet function, $\psi_{j,n}(t)$, and $W_{j,n}$ are the wavelet coefficients. The parameter n (translation parameter) shifts the wavelet in time and the parameter $s = 2^j$ (scale parameter) controls the wavelet frequency bandwidth, hence the resulting joint time–frequency analysis.

Compared to its "continuous" version that cannot be performed in real-time, the discrete wavelet transform is computationally efficient because of the existence of a fast orthogonal wavelet transform algorithm based on a set of filter banks [21]. In Mallat's filter bank tree, the discrete wavelet transform decomposition is done by pairs of low-pass and high-pass filters. Each level of decomposition, j, corresponds to a frequency band $f_j \pm \Delta f_j/2$. The central frequency, f_j, is a function of the mother wavelet central frequency, F, and the signal sampling rate Δ, through

$$f_j = \frac{\Delta \times F}{2^j}. \tag{6}$$

The bandwidth, Δf_j, can be normally estimated as half of the distance between adjacent central frequencies. Considering Eq. (6), this quantity can thus be written as

$$\Delta f_j = \left|\frac{f_{j+1} - f_{j-1}}{2}\right| = \frac{3}{4} f_j. \tag{7}$$

De-nosing and compression of the original signal can be achieved if only a few wavelet coefficients containing the essential information of interest are retained and the remaining coefficients, related to unnecessary information such as noise, are discarded. This is obtained by a "pruning" process followed by a "thresholding" process [8]. In the pruning process, coefficients in one or more decomposition levels, corresponding to the frequency band of interest, are retained according to Eqs. (6) and (7). In the thresholding process, only those coefficients whose amplitude exceeds a certain threshold value are further retained. One simple way to define such threshold is based on a percentage of the maximum coefficient amplitude.

It is important to emphasize that the success of a proper discrete wavelet transform decomposition is dependent on choosing a mother wavelet that best matches the shape of the signal that is being analyzed. In the present work, the Daubechies mother wavelet of order 40 was adopted due its similarity to the narrowband ultrasonic signals to be analyzed [15,16]. The sixth decomposition detail level was chosen for pruning and thresholding as the one that most closely represented the frequency band of interest.

4. Application to damage detection in multi-wire strands

The general algorithm proposed in this study can be divided in three part steps and is illustrated in the flowchart of Fig. 1. Guided ultrasonic wave signals are processed through the discrete wavelet transform. After pruning and thresholding, the representative wavelet coefficients are retained. A damage index is computed from certain features extracted from the representative wavelet coefficients. The damage index is a scalar in the univariate case (one feature), and a vector in the multivariate case (multiple features). An outlier analysis is performed to determine whether a current damage index is representative of damage or it is simply within the baseline, undamaged distribution.

This general approach is applicable to many structural components having waveguide geometry (e.g. plates, rods, pipes) and thus lending themselves to guided ultrasonic wave propagation. Depending on the specific application, the ultrasonic configuration (whether pulse-echo or pitch-catch), the discrete wavelet transform decomposition levels, as well as the features considered in the computation of the damage index may change.

In this paper the approach is demonstrated for the health monitoring of seven-wire steel strands used in prestressed concrete structures and cable-stayed or suspension bridges. Several previous works have demonstrated that the strand geometry lends itself to guided ultrasonic wave testing, which has been used for detecting damage and for measuring applied loads in these components [14,22–28].

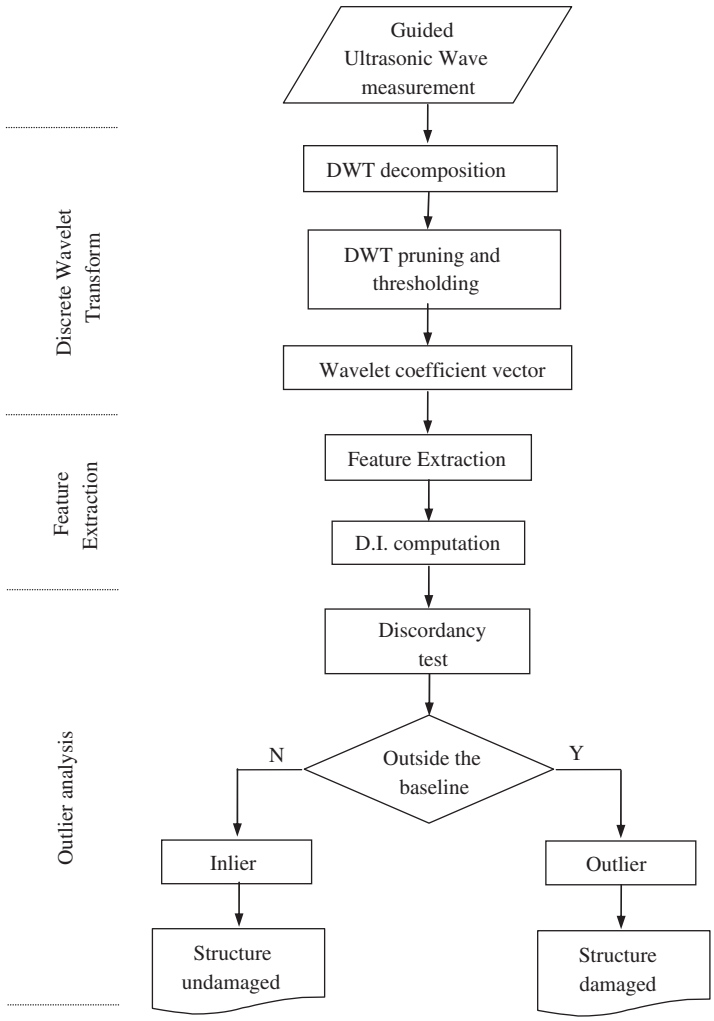

Fig. 1. Flowchart of the proposed strategy for damage detection based on discrete wavelet transform feature extraction and outlier analysis.

4.1. Experimental setup

The test component under investigation was a conventional high-grade steel 270, seven-wire twisted strand with a diameter of 15.24 mm (0.6 in). A notch was machined in one of the six peripheral wires by saw-cutting with depths ranging from 0.5 to 3 mm. A final cut resulted in the complete fracture of the helical wire, which was the largest defect examined within a total of six different defect sizes. It should be pointed out that the geometry of the saw was such that cutting the individual wire at the depth of 3 mm also produced small indentations into the two adjacent wires. The notches were machined perpendicular to the strand axis. Fig. 2a illustrates the defect sizes examined. In Fig. 2b is the corresponding reduction in the strand's cross-sectional area.

The strand was subjected to a 120 kN tensile load, corresponding to 45% of the material's ultimate tensile strength, that is a typical operating load for stay cables. The load was applied in the laboratory test by a hydraulic jack. As shown in Fig. 2c, a pair of magnetostrictive sensors, resonant at 320 kHz, was used to excite and detect guided ultrasonic waves. The 320 kHz frequency was chosen as a low attenuation value for loaded strands [14]. The distance d_1 between the transmitting magnetostrictive sensor and the receiving magnetostrictive sensor, as well as the distance d between the receiving magnetostrictive sensor and the notch, were fixed at 203 mm (8 in). The receiver detected the signal propagating directly from the transmitter (direct signal) and any echo reflected from the notch (defect reflection).

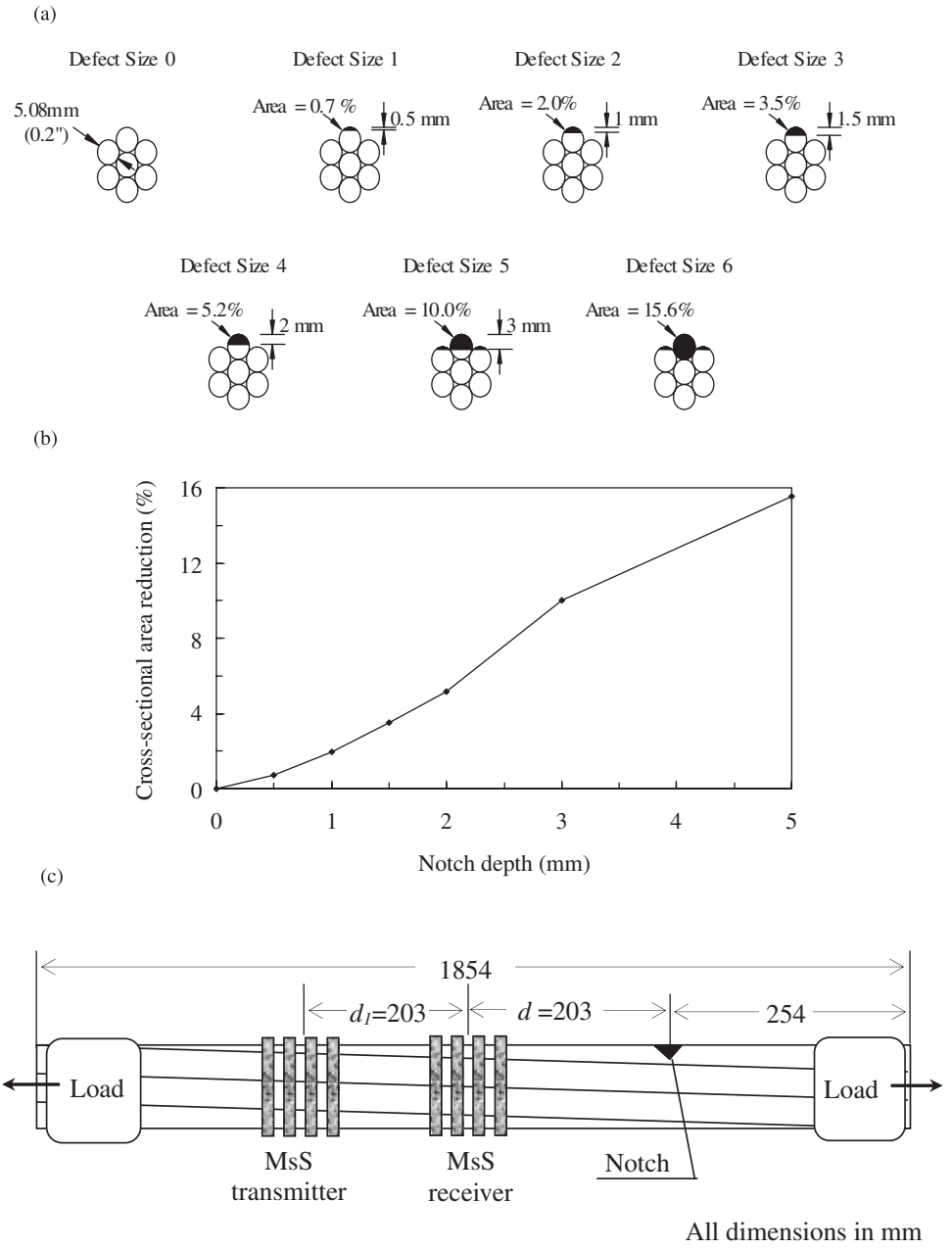

Fig. 2. (a) The different notch depths examined; (b) reduction of the cross-sectional area of the strand as a function of notch depth; and (c) schematic representation of the experimental setup.

A National Instruments PXI© unit running under LabVIEW© was employed for signal excitation, detection and acquisition. Five-cycle tonebursts (50 V peak-to-peak) centered at 320 kHz, modulated with a triangular window, were used as generation signals. The acquisition sampling rate was 33 MHz.

4.2. Wavelet coefficient analysis

An example of the discrete wavelet transform processing adopted in this study is shown in Fig. 3, which refers to the monitoring of the 2-mm-deep notch. The signals were first acquired after 50 digital averages. Two

time windows were selected for the direct signal and the defect reflection. The direct signal window was fixed between 35 and 97 μs for the given constant transmitter–receiver distance and it consisted of 2048 points (Fig. 3a). The defect reflection window consisted of 4096 points and covered the expected arrival of the reflection (Fig. 3b). Clearly, in a practical application where the defect location is not known a priori, the second window must be large enough to cover the range of possible locations of a defect. In turn, the maximum distance at which a given-size defect can be detected will be determined by the frequency-dependent guided ultrasonic wave attenuation losses and by the de-noising performance of the discrete wavelet transform processing. Notice that the scale amplitude of the defect reflection in Fig. 3b is set to one order of magnitude smaller than that of the direct signal in Fig. 3a. The corresponding wavelet coefficient vectors at

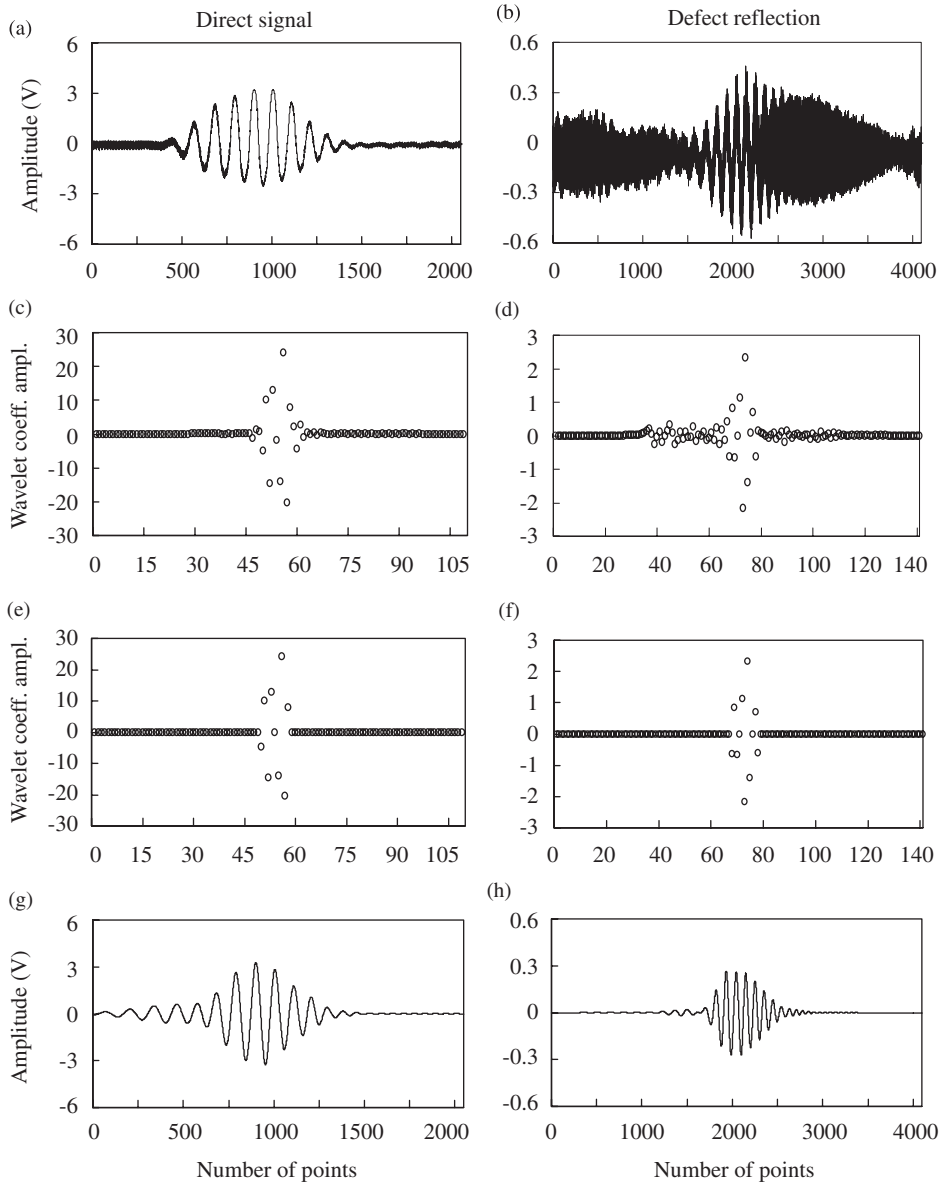

Fig. 3. (a) Direct signal; (b) reflection from 2-mm-deep notch; (c) wavelet coefficient vector at level 6 for direct signal; (d) wavelet coefficient vector at level 6 for defect reflection; (e) wavelet coefficient vector at level 6 for direct signal after 20% thresholding; (f) wavelet coefficient vector at level 6 for defect reflection after 20% thresholding; (g) reconstructed direct signal; and (h) reconstructed defect reflection.

decomposition level 6 are shown in Fig. 3c and d, respectively. Since the number of points of the original signals differs, the size of the two wavelet coefficient vectors differs as well (109 versus 141). Most of the wavelet coefficients in Fig. 3c and d have very low amplitude and thus do not carry any information on the signal of interest; these can be eliminated by setting a threshold equal to 20% of the maximum coefficient amplitude. The thresholded coefficient vectors are shown in Fig. 3e and f for the direct signal and the defect reflection, respectively. The time-domain signals reconstructed from these vectors are shown in Fig. 3g and h, confirming that only few wavelet coefficients sufficiently represent the information of interest. The extraction of the wavelet coefficients from the time-domain signals is done in pseudo-real time owing to the efficiency of the discrete wavelet transform algorithm.

The fact that the size of the wavelet coefficient vectors (109 and 141) does not follow the dyadic decomposition rule (2^n points) is due to the so-called ''boundary problem''. The perfect dyadic decomposition is only achieved when the Haar mother wavelet is employed. Other mother wavelets spill over the signal time windows creating spurious wavelet coefficients at the start and at the end of the windows.

The threshold chosen to select the relevant wavelet coefficients is an important variable that ultimately affects the sensitivity to defect size. The 20% threshold in Fig. 3 was chosen based on simple visual observation of the decomposition level 6. Other procedures, based on statistical analysis, exist for selecting this threshold [21]. For the results that follow, a more severe threshold was used for the defect reflection portion of the signal, where de-noising is more critical. The result of a more severe threshold is an increase in sensitivity to defect size. The specific threshold combination used was 20% and 70% for the direct signal and for the defect reflection, respectively.

4.3. Damage index and feature selection

The proposed damage index is the ratio between certain features of the defect reflection, $F_{\text{reflection}}$, and the same features of the direct signal, F_{direct}:

$$\text{Damage index} = \frac{F_{\text{reflection}}}{F_{\text{direct}}}. \tag{8}$$

Normalizing the defect reflection by the direct signal eliminates any dependence of the monitoring result on the signal power to the transmitter or on the sensor/strand electro-mechanical coupling efficiency. If a defect is a perfect reflector of the ultrasonic energy, the damage index is 1. For the notch defects examined in this study, the damage index will be smaller than one since only a small portion of the incoming signal will be reflected.

The features used were computed from the wavelet coefficient vectors after pruning and thresholding as described in the previous section. These were the variance, the root mean square, the maximum amplitude and the peak-to-peak amplitude. The effectiveness of these features for damage detection and sizing is well known [10,16].

4.4. Outlier analysis

4.4.1. Noise corruption

The baseline distribution of the damage indices was constructed by corrupting a guided ultrasonic wave measurement, averaged over ten acquisitions, by two different levels of white Gaussian noise. The noise signals were created by the MATLAB *randn* function. The *randn* function generates arrays of random numbers whose elements are normally distributed with zero mean and standard deviation equal to 1. The function was pre-multiplied by a factor that determines the noise level. Factors equal to 0.01 and 0.1 were considered as ''low noise'' and ''high noise'', respectively. For each noise level, 300 baseline samples were created. The same approach was taken to generate a large number of data for the damaged conditions. The ten-average signals acquired for each of the six defect sizes were thus corrupted by the low noise level and the high noise level, generating a total of 300 samples for each damage size and noise level. This procedure was adopted for both the univariate and the multivariate analyses. Thus Monte Carlo simulation was not used in either analyses.

As an example, the ten-average direct signal and reflection from the 3-mm-deep notch are shown in Fig. 4a and b, respectively. Typical noise traces are illustrated in Fig. 4c and d (low noise) and in Fig. 4e and f

(high noise). Notice the different scale in the ordinate axis between the two noise levels (the high noise is about ten times larger than the low noise). Fig. 4g and h show the corrupted ultrasonic signals that were opportunely offset for clarity of presentation.

The added noise can be quantified in terms of signal-to-noise ratio by the following expression:

$$\text{Signal-to-noise ratio (dB)} = 10\ \text{Log}\left(\sum_{i=1}^{N} s_i^2/N \Big/ \sum_{i=1}^{N} u_i^2/N\right), \tag{9}$$

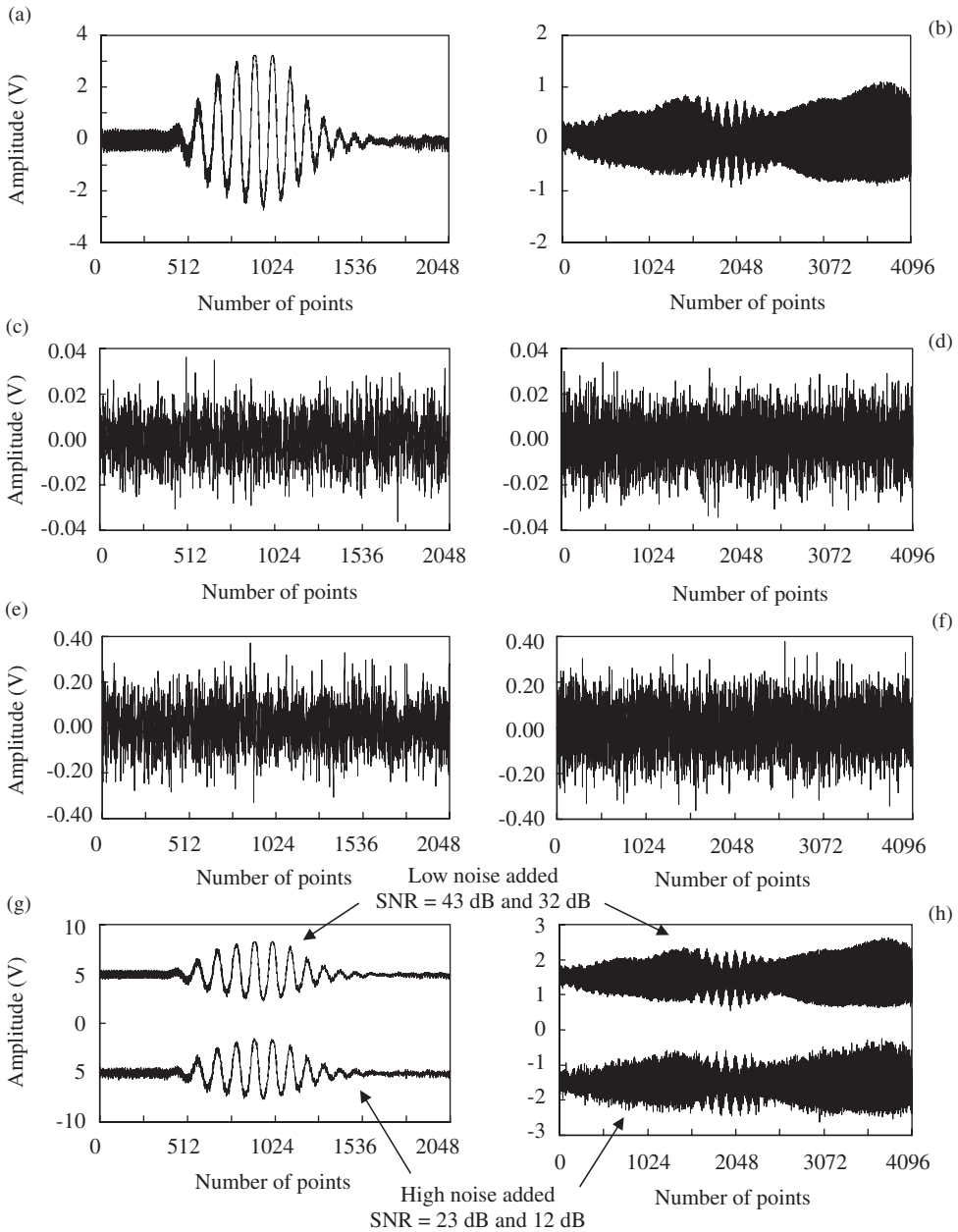

Fig. 4. (a) Direct signal; (b) reflection from 3-mm-deep notch; (c) low level noise for the direct signal; (d) low level noise for the reflection; (e) high level noise for the direct signal; (f) high level noise for the reflection; (g) corrupted direct signals; and (h) corrupted reflection signals.

where s_i and u_i are the amplitudes of the ultrasonic signal and the noise signal, respectively, and N is the number of points. The signal-to-noise ratio between the direct signal and the two 0.01 and 0.1 noise levels was about 43 and 23 dB, respectively. The signal-to-noise ratio between the reflection from the 3-mm-deep notch and the two 0.01 and 0.1 noise levels was about 32 and 12 dB, respectively. Clearly, the latter two values decreased with decreasing notch depth.

4.4.2. Univariate analysis for low noise

In this section is the outlier analysis results when the four features of variance, root mean square, maximum amplitude and peak-to-peak amplitude of the wavelet coefficients were considered separately. The damage index in Eq. (8) is thus a scalar.

Fig. 5 illustrates the deviation statistics z_ζ of the damage index variance of the baseline for signals corrupted with the low noise level of 0.01. The mean and the standard deviation of all 300 damage index variances were computed, and the inclusive deviation was computed for each of the baseline samples from Eq. (1). The horizontal line is the value of 2.655 representing the 99.73% confidence threshold. It can be seen that as few as three baseline samples exceed the threshold and thus classify as outliers. In the context of the present framework, these values represent false damage indications (false positives).

Fig. 6 summarizes the deviation statistics of the same damage index variance for the baseline and for all damage conditions, still in the low noise level case. The logarithmic scale is used in the graph. Each value was obtained from Eq. (1) where the mean and the standard deviation are those of the baseline. Thus the exclusive method was adopted, simulating an unsupervised learning approach where the damage conditions are unknown a priori. The threshold value in Fig. 6 is obviously the same as in Fig. 5. Clear steps can be seen in the discordancy plot at sample numbers 301, 601, 901, 1201, 1501 and 1801, corresponding to the progressive reduction of the strand's cross-sectional area as described in Fig. 2b. For the 0.5-mm-deep notch, equivalent to less than 1% reduction in cross-sectional area, there are only four inliers, i.e. false negative indications, with the remaining 296 samples properly indicating damaged conditions. All other damage sizes, between sample numbers 601 and 2100 and corresponding to more than 2% cross-sectional area reduction, are properly classified as damaged conditions. Overall the results are very satisfactory confirming the effectiveness of the wavelet coefficient variance feature for computing the damage index.

By applying the same routine to the other three features, and thus computing the damage index from the root mean square, maximum, and peak-to-peak amplitude of wavelet coefficients, the results in Fig. 7 were obtained. It should be noted that the qualitative trend of increasing discordancy with increasing defect size is the same as in Fig. 6. However, it can be seen that the sensitivity to damage (represented by the rate of change of the discordancy plot) is larger for the variance-based damage index than it is for any of the other three features. The damage index maximum and peak-to-peak amplitude cannot be used to discriminate between the 0.5 and the 1.0 mm notch depths. This is due to the fact that the differences between such small defects lie in a few wavelet coefficients of lower amplitude that do not affect the extreme values, but do affect both the variance and the root mean square values. Interestingly, the damage index peak-to-peak amplitude is the only

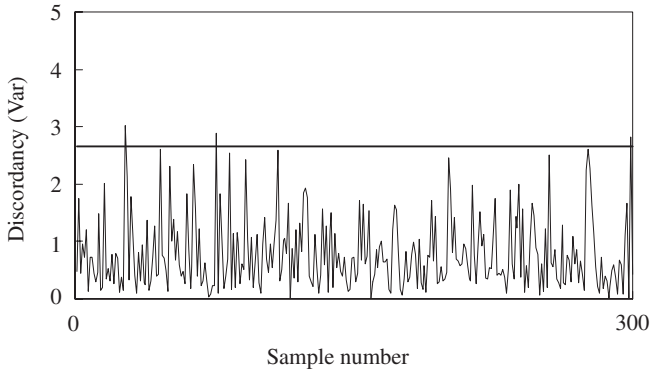

Fig. 5. Discordancy test for the feature damage index variance. Baseline (undamaged) data corrupted with the low level noise.

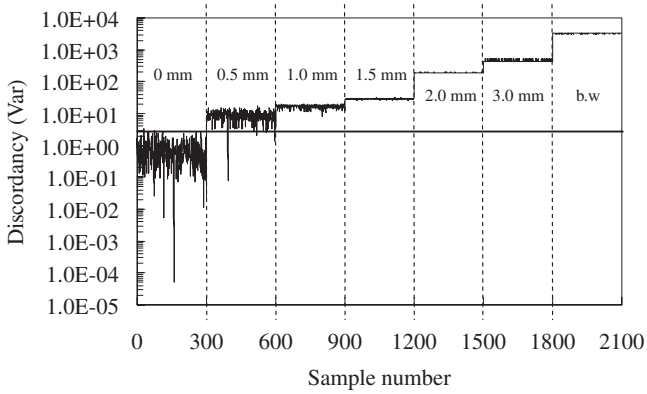

Fig. 6. Discordancy test for the feature damage index variance. Baseline (undamaged) and damaged data corrupted with the low level noise.

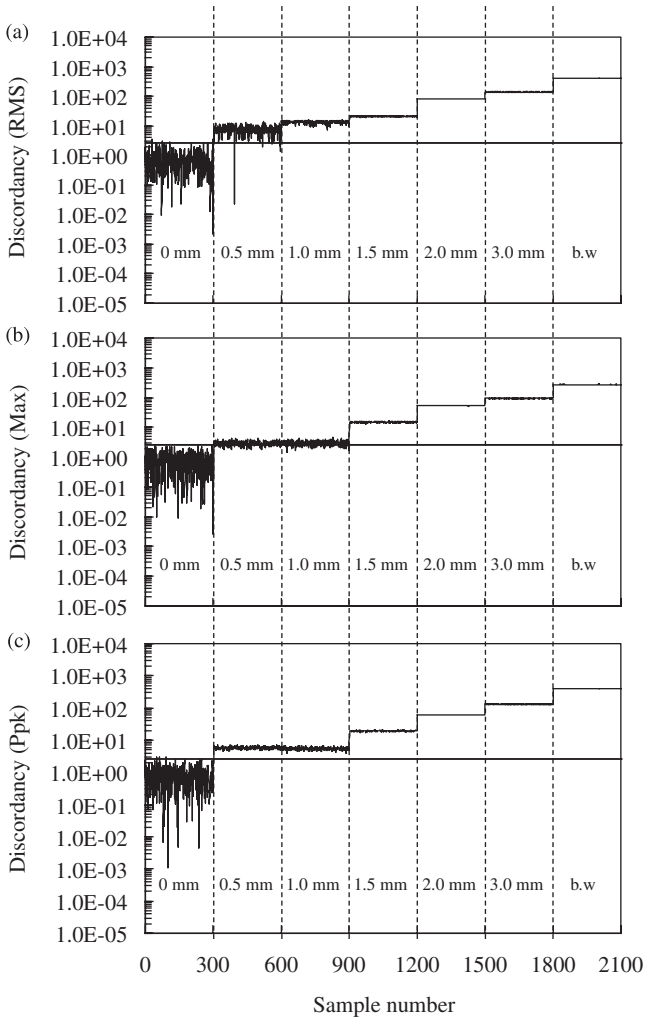

Fig. 7. Discordancy test for the baseline (undamaged) and damaged data corrupted with the low level noise damage index computed from the following features: (a) root means square; (b) maximum; and (c) peak-to-peak amplitude.

feature resulting in no false negative indications, with all samples between 301 and 2100 being properly recognized as damaged conditions.

4.4.3. Univariate analysis for high noise

In Fig. 8 is a plot of the variance-based damage index obtained for the baseline and all damage conditions in the presence of the high noise level of 0.1. The 99.73% confidence threshold value, the horizontal line in the figure, is now equal to 2.584. Within the 300 baseline samples, only three are outliers and thus false positives. Compared to the results of Fig. 6, the first discordancy step now occurs at sample number 1201 for the 2.0-mm-deep notch. Thus, only cross-sectional reductions above 5% are properly classified as damaged conditions in the presence of the high noise level. There are no false negative indications in this range. Below 5% cross-sectional reduction, only one sample is properly classified as an outlier at the 1.5 mm notch depth where the signal-to-noise ratio between the defect reflection and the noise level was around 7.5 dB.

It can also be seen that the sensitivity to damage (rate of change of the discordancy plot) is reduced in the high noise case compared to the low noise case. This is a result of the larger standard deviation of the baseline that reduces the value of the deviation statistics, Eq. (1).

The results from the other features considered separately, not shown here, are similar to those presented in Fig. 8. Every feature enables the detection of damage above 5% cross-sectional area reduction, with no false negative indications. The obvious conclusion from these results is that an elevated level of noise reduces the ability to detect the presence of the smaller defects.

Table 1 compares the 99.73% confidence thresholds computed from the baseline data for each of the features and for the two noise levels. It can be seen that the threshold is not substantially affected by the specific feature or noise level considered. Table 2 summarizes the results of all univariate cases examined including those in Figs. 6–8. The number of outliers relative to 300 samples is reported for each of the features and the two levels of noise. These outliers are false positive indications for the baseline data (damage size 0 in Table 2), whereas they correctly indicate anomalous conditions for the defect data. Comparing the different features, the damage index peak-to-peak amplitude performs the best in terms of robustness of the damage detection; it gives no false negatives for the low noise level, and properly classifies the largest number of defect samples for the high noise level. In contrast, the damage index maximum feature shows the worst performance in robustness since it properly classifies the lowest number of defect samples. The damage index variance retains the largest sensitivity to damage size in terms of rate of change of the discordancy values.

4.4.4. Multivariate analysis for low noise

The four wavelet-based features considered separately in the previous two sections were subsequently used simultaneously to construct a four-dimensional damage index vector for the outlier analysis. The deviation statistics is now replaced by the Mahalanobis squared distance expressed in Eq. (4).

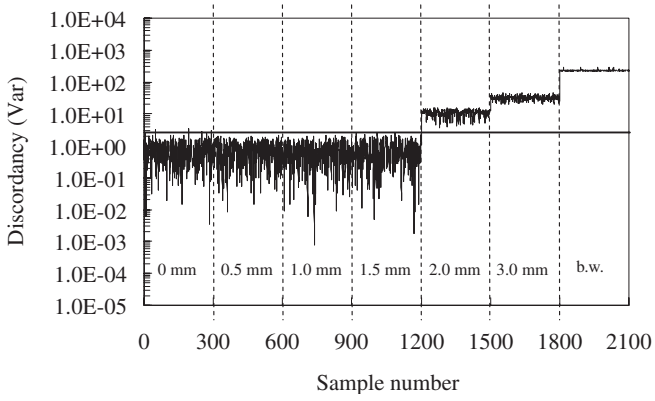

Fig. 8. Discordancy test for the feature damage index variance. Baseline (undamaged) and damaged data corrupted with the high level noise.

Table 1
Univariate analysis: threshold values for each feature and the two levels of added noise

Feature	Corruption level	Threshold
D.I. (Var)	0.01	2.6551
D.I. (Var)	0.1	2.5482
D.I. (RMS)	0.01	2.6661
D.I. (RMS)	0.1	2.5425
D.I. (Max)	0.01	2.5851
D.I. (Max)	0.1	2.9102
D.I. (Ppk)	0.01	2.5914
D.I. (Ppk)	0.1	2.6299

D.I.: damage index; Var, variance; RMS, root mean square; Max: maximum; Ppk, peak-to-peak.

Table 2
Univariate analysis: number of outliers $n/300$ for the various damage sizes and the two levels of added noise

Feature/corruption level	Damage size (notch depth (mm))						
	0	0.5	1.0	1.5	2.0	3.0	5.0 (b.w.)
D.I. (Var)/0.01	3/300	296/300	300/300	300/300	300/300	300/300	300/300
D.I. (Var)/0.1	4/300	0/300	0/300	1/300	300/300	300/300	300/300
D.I. (RMS)/0.01	6/300	296/300	300/300	300/300	300/300	300/300	300/300
D.I. (RMS)/0.1	3/300	1/200	4/300	0/300	300/300	300/300	300/300
D.I. (Max)/0.01	1/300	225/300	225/300	300/300	300/300	300/300	300/300
D.I. (Max)/0.1	0/300	0/300	0/300	0/300	300/300	300/300	300/300
D.I. (Ppk)/0.01	4/300	300/300	300/300	300/300	300/300	300/300	300/300
D.I. (Ppk)/0.1	2/300	11/300	10/300	16/300	300/300	300/300	300/300

D.I.: damage index; Var, variance; RMS, root mean square; Max: maximum; Ppk, peak-to-peak.

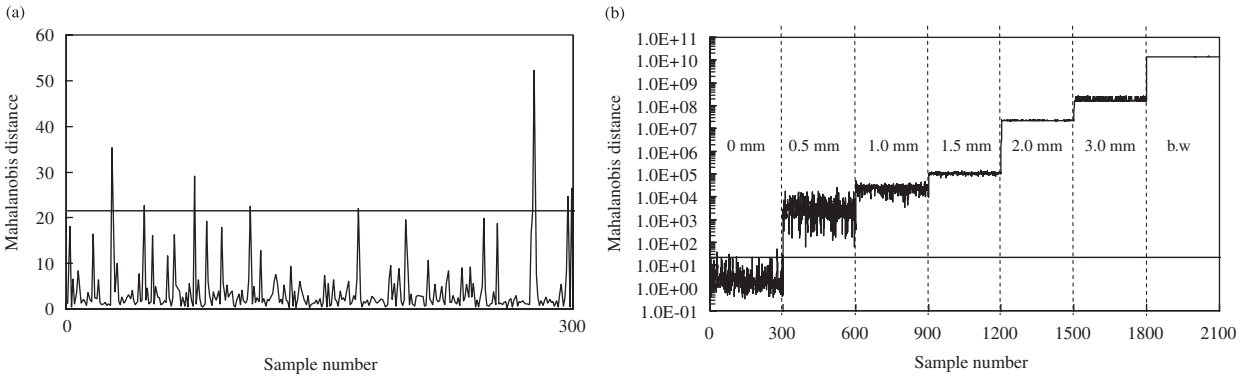

Fig. 9. (a) Mahalanobis squared distance for the baseline (undamaged) data corrupted with the low level noise and (b) Mahalanobis squared distance for the baseline (undamaged) and damaged data corrupted with the low level noise.

Fig. 9a illustrates the Mahalanobis squared distance calculated on the baseline data for the low noise level of 0.01. The mean vector and the covariance matrix were determined from the 300 damage index vectors associated with the undamaged condition of the strand. Each baseline vector was then compared to the mean vector and the covariance matrix by using Eq. (4). The horizontal line in this figure represents the 99.73% confidence threshold value of 21.579, which is one order of magnitude larger than the corresponding

thresholds of the univariate cases (Table 1). It can be seen in Fig. 9a that eight baseline samples are outliers, thus false positive indications.

The Mahalanobic squared distance of all samples, including the baseline data and the damage data, are summarized in Fig. 9b. As for the univariate analyses, the discordancy values of the damaged conditions were calculated in an exclusive manner. The same stepwise trend observed in the univariate cases is seen in this figure. However, the multivariate analysis outperforms any of the univariate results at the same level of noise corruption. First, all damaged conditions are properly classified as outliers, thus there are no false negative indications. Second, the values of the Mahalanobic squared distances for the damage data are several orders of magnitude larger than the corresponding values of the univariate deviation statistics. For example, the Mahalanobic squared distance for the 2-mm-deep notch data shown in Fig. 9b are five orders of magnitude larger than the deviation statistics in Figs. 6 and 7. As a consequence, the sensitivity to damage is considerably improved. Finally, the Mahalanobic squared distance values provide good discrimination between all defect sizes, including the smallest notch depths.

In summary, results in Fig. 9b confirm that it is advantageous to combine multiple guided ultrasonic wave features to provide a large sensitivity to the defects. Nevertheless, compared to previous multivariate outlier analyses in structural monitoring applications, the dimension of the damage index vector is still kept at a very low value by selecting only four features of the guided ultrasonic wave signals containing the essential information of interest.

4.4.5. Multivariate analysis for high noise

Following the same approach, the Mahalanobic squared distance results of the four-dimensional damage index vectors corrupted with the high noise level of 0.1 are shown in Fig. 10. The 99.73% confidence threshold was now computed as 18.137. Fig. 10a refers to the baseline results, and Fig. 10b summarizes the baseline and the damaged cases results. Compared to the low noise results of Fig. 9, it is clear that the heavier noise corruption compromises the ability to detect the notch depths below 2.0 mm, corresponding to a 5% reduction in strand's cross-sectional area. The same result was found from the prior univariate analyses. The ratios of correctly classified outliers below 5% area reduction are only 12/300, 7/300 and 1/300 for notch depths of 0.5, 1.0 and 1.5 mm, respectively. Above the 5% area reduction, the sensitivity to defect detection is also degraded with the increasing noise level; for example, the Mahalanobic squared distance values for the 2 mm notch depth in Fig. 10b are four orders of magnitude smaller than the corresponding values in Fig. 9b. The reduced number of false positive indications (three against eight) is the only improvement over the low noise level.

The effectiveness of the results in Fig. 10 must be appreciated in comparison with the univariate results in Fig. 8 for the same noise level. The improvement in defect detection sensitivity from considering multiple features is substantial; for example, the Mahalanobic squared distance values for the 2-mm-deep notch in the multivariate analysis are two orders of magnitude larger than the corresponding values of the univariate deviation statistics.

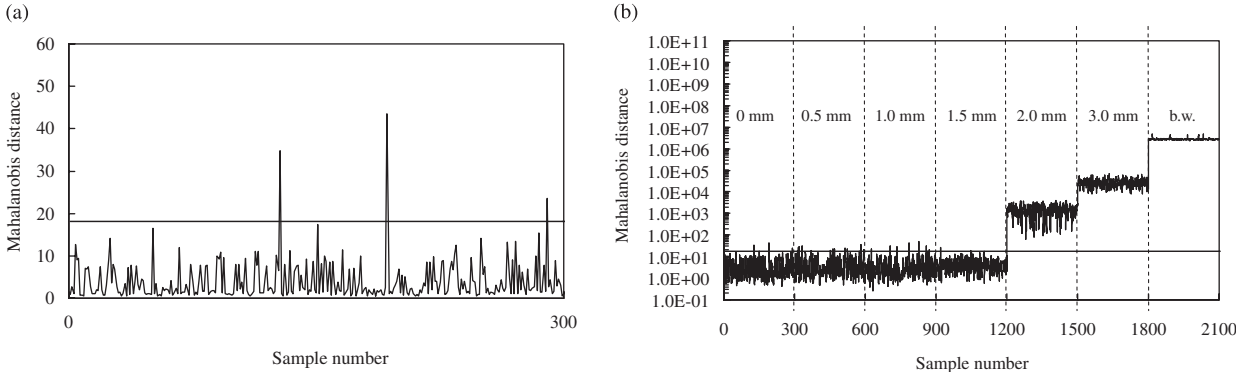

Fig. 10. (a) Mahalanobis squared distance for the baseline (undamaged) data corrupted with the high level noise and (b) Mahalanobis squared distance for the baseline (undamaged) and damaged data corrupted with the high level noise.

Table 3
Multivariate analysis (four features): number of outliers $n/300$ for the various damage sizes and the two levels of added noise

Corruption level	Damage size (notch depth (mm))						
	0	0.5	1.0	1.5	2.0	3.0	5.0 (b.w.)
0.01	8/300	300/300	300/300	300/300	300/300	300/300	300/300
0.1	3/300	12/300	7/300	1/300	300/300	300/300	300/300

Table 4
Multivariate analysis (two features): number of outliers $n/300$ for the various damage sizes and the two levels of added noise

Corruption level	Damage size (notch depth (mm))						
	0	0.5	1.0	1.5	2.0	3.0	5.0 (b.w.)
0.01	14/300	300/300	300/300	300/300	300/300	300/300	300/300
0.1	7/300	8/300	5/300	8/300	300/300	300/300	300/300

In Table 3 are the number of outliers detected in the multivariate analyses for both levels of noise considered. As in Table 2, the outliers are false positive indications for the baseline data (damage size 0) and, instead, correct indications of anomalies for the defect data.

4.4.6. Multivariate analysis for two-dimensional problem

Outlier analyses were also conducted by reducing the dimension of the damage index vector from four to two. The two features considered were the variance and the peak-to-peak amplitude of the representative wavelet coefficients. As discussed above, these two features produced the best results of all univariate analyses, respectively, in terms of sensitivity to damage size (largest rate of change of the discordancy values) and robustness of damage detection (largest number of damage samples correctly classified as outliers).

The Mahalanobis squared distance results, only summarized here in Table 4, showed a performance that was expectedly between the straight univariate analyses and the four-dimensional multivariate analysis. As seen in this table, the analysis was able to correctly classify all damage sizes for the low noise level, and all notches above the 2.0-mm depth (5% area reduction) for the high noise level. Compared to the univariate cases, the two-dimensional analysis provided an increase in defect sizing sensitivity of at least one order of magnitude. However, the increase in sensitivity was smaller than with the four-dimensional analysis. For example, in the low noise level the two-dimensional Mahalanobis squared distance values for the 2-mm-deep notch were two orders of magnitude larger than the univariate deviation statistics (compared to the five orders of magnitude of the four-dimensional Mahalanobis squared distance). For the high noise level, the two-dimensional Mahalanobis squared distance improvement over the univariate deviation statistics was one order of magnitude (compared to the two orders of magnitude of the four-dimensional Mahalanobis squared distance).

5. Discussion and conclusions

In this paper a technique that is a combination of the known concepts of discrete wavelet transform and outlier analysis for structural health monitoring based on guided ultrasonic waves is described. Guided waves are ideal candidates for monitoring any structural component that has a finite cross-sectional geometry. Guided wave methods offer larger monitoring ranges compared to "local" methods such as conventional ultrasonic testing, and larger sensitivity to smaller defects compared to "global" methods such as modal testing. The specific application of interest in this study is the detection of defects in multi-wire steel strands based on the reflections of guided waves that are excited and detected by a pair of magnetostrictive ultrasonic transducers.

A damage index was constructed based on certain features of the discrete wavelet decomposition of the time-domain ultrasonic signals. These features, obtained after pruning and thresholding procedures, compress the signals to the essential defect-sensitive information. The wavelet-based features were then used in a conventional outlier analysis both individually (univariate case) and collectively (multivariate case). The population of data for the outlier analysis was created by adding two different levels of digital random noise to the ultrasonic measurements. The low noise level corresponded to signal-to-noise ratios of 43 and 32 for the direct signal and the reflection from a 3-mm-deep notch, respectively. The corresponding signal-to-noise ratios for the high noise level were 23 and 12, respectively. A total of 300 samples were thus obtained for the baseline, undamaged condition and for each of the damage conditions. These consisted of six different notch depths ranging from a 0.7% to a 15.6% reduction in the strand's cross-sectional area.

The outlier analysis, conducted with a 99.73% confidence threshold, successfully detected all damage conditions in the low noise case, and all damage larger than 5% strand area reduction in the high noise case. The different performance was due to the increased dispersion of the baseline distribution with increasing noise level. It was further shown that combining multiple features in a multivariate analysis substantially improves the performance in terms of sensitivity to defect detection and discrimination among the different defect sizes. Nevertheless, by considering the sensitive wavelet-based features, the dimension of the multivariate analysis was still kept at a minimum, as desirable for on-line, continuous monitoring. By combining as few as two features, the improvement in defect detection and discrimination was at least of one order of magnitude compared to either feature considered individually. The improvement increased to several orders of magnitude when as many as four features were combined.

In a given monitoring application, the choice of the number of features to consider in the multivariate analysis should be a compromise between the desired defect detection performance and the required speed of the analysis within the available computational resources. The results presented here strictly apply to ungrouted strands and notch-like defects located at 203 mm from the sensing magnetostrictive coil. There are at least two practical instances when defects might be searched within this short range from the sensing coil: the monitoring of the strand's critical anchored regions that are prone to corrosion and stress concentrations, and the use of multiple coils that are closely spaced for covering an extended length of a strand. For grouted strands or when defects are searched at larger distances from the sensing coil, the defect detection performance will be somewhat poorer due to the degraded signal-to-noise ratios of the measurements. In these cases adjustments may be needed in the wavelet amplitude thresholds or in the number of averages computed on the raw signals prior to the analysis. It should also be mentioned that problems will arise if defects are located too close to the receiving coil, in which case the direct signal and the defect reflection may overlap. Finally, artificial noise corruption only accounts for some of the baseline variability that would be encountered in a practical application. However, the concept of using essential wavelet-based features of guided ultrasonic waves for a low-dimension outlier analysis should be appealing in many structural monitoring applications.

Acknowledgments

This research was funded by the National Science Foundation Grant CMS-0221707, the California Department of Transportation contract 59A0538 and by the UCSD/Los Alamos Cooperative Agreement for Research and Education (CARE). Elisa Sorrivi performed this research while visiting UC San Diego under a Study Abroad Fellowship of the University of Bologna's School of Engineering. Ivan Bartoli at UC San Diego is acknowledged for preparing Fig. 2a.

References

[1] V. Barnett, T. Lewis, *Outliers in Statistical Data*, Wiley, New York, 1994.
[2] K. Worden, Structural fault detection using a novelty measure, *Journal of Sound and Vibration* 201 (1997) 85–101.
[3] K. Worden, G. Manson, N.R.J. Fieller, Damage detection using outlier analysis, *Journal of Sound and Vibration* 229 (2000) 647–667.
[4] K. Worden, S.G. Pierce, G. Manson, W.R. Philp, W. Staszewski, B. Culshaw, Detection of defects in composite plates using Lamb waves and novelty detection, *International Journal of System Science* 31 (2000) 1397–1409.

[5] G. Manson, K. Worden, Experimental validation of a structural health monitoring methodology. Part II. Novelty detection on a gnat aircraft, *Journal of Sound and Vibration* 259 (2003) 345–363.
[6] S.E. Guttormsson, R.J. Marks Jr., M.A. El-Sharkawi, Elliptical novelty grouping for on-line short-turn detection of excited running rotors, *IEEE Transactions on Energy Conversion* 14 (1999) 16–22.
[7] P. Omenzetter, J.M.W. Brownjohn, P. Moyo, Identification of unusual events in multi-channel bridge monitoring data, *Mechanical System and Signal Processing* 18 (2004) 409–430.
[8] A. Abbate, J. Koay, J. Frankel, S.C. Schroeder, P. Das, Signal detection and noise suppression using a wavelet transform signal processor: application to ultrasonic flaw detection, *IEEE Transactions on Ultrasonic, Ferroelectrics, and Frequency Control* 44 (1997) 14–26.
[9] W. Staszewski, G. Pierce, K. Worden, W. Philp, G. Tomlinson, B. Culshaw, Wavelet signal processing for enhanced Lamb-wave defect detection in composite plates using optical fiber detection, *Optical Engineering* 36 (1997) 1877–1888.
[10] W. Staszewski, C. Boller, G. Tomlinson, *Health Monitoring of Aerospace Structures*, Wiley, Munich, Germany, 2004.
[11] W. Staszewski, Intelligent signal processing for damage detection in composite materials, *Composites Science and Technology* 62 (2002) 941–950.
[12] C.A. Paget, S. Grondel, K. Levin, C. Delebarre, Damage assessment in composites by Lamb waves and wavelet coefficients, *Smart Materials and Structures* 12 (2003) 393–402.
[13] J. McNamara, F. Lanza di Scalea, Improvements in non-contact ultrasonic testing of rails by the discrete wavelet transform, *Materials Evaluation* 62 (2004) 365–372.
[14] P. Rizzo, F. Lanza di Scalea, Load measurement and health monitoring in cable stays via guided wave magnetostrictive ultrasonics, *Materials Evaluation* 62 (2004) 1057–1065.
[15] P. Rizzo, F. Lanza di Scalea, Ultrasonic inspection of multi-wire steel strands with the aid of the wavelet transform, *Smart Materials and Structures* 14 (2005) 685–695.
[16] P. Rizzo, F. Lanza di Scalea, Wavelet-based feature extraction for automatic defect classification in strands by ultrasonic structural monitoring, *Smart Structures and Systems* 2 (2006) 253–274.
[17] P. Rizzo, I. Bartoli, A. Marzani, F. Lanza di Scalea, Defect classification in pipes by neural networks using multiple guided ultrasonic wave features, *ASME Journal of Pressure Vessel Technology* 127 (2005) 294–303.
[18] F. Lanza di Scalea, P. Rizzo, S. Coccia, I. Bartoli, M. Fateh, E. Viola, G. Pascale, Non-contact ultrasonic inspection of rails and signal processing for automatic defect detection and classification, *Insight—Non-Destructive Testing and Condition Monitoring* 47 (2005) 346–353.
[19] K. Worden, H. Sohn, C.R. Farrar, Novelty detection in a changing environment: regression and interpolation approaches, *Journal of Sound and Vibration* 258 (2002) 741–761.
[20] G. Manson, G. Pierce, K. Worden, T. Monnier, P. Guy, K. Atherton, Long-term stability of normal condition data for novelty detection, *Proceedings of SPIE, Seventh International Symposium of Smart Structures and Materials,* Newport Beach, CA, 2000, pp. 323–334.
[21] S.G. Mallat, *A Wavelet Tour of Signal Processing*, Academic Press, New York, 1999.
[22] H. Kwun, C.M. Teller, Nondestructive evaluation of steel cables and ropes using magnetostrictively induced ultrasonic waves and magnetostrictively detected acoustic emissions, US Patent No. 5,456,113, 1995.
[23] H. Kwun, K.A. Bartels, J.J. Hanley, Effect of tensile loading on the properties of elastic-wave propagation in a strand, *Journal of the Acoustical Society of America* 103 (1998) 3370–3375.
[24] H.-L. Chen, K. Wissawapaisal, Measurement of tensile forces in a seven-wire prestressing strand using stress waves, *ASCE Journal of Engineering Mechanics* 127 (2001) 599–606.
[25] B.N. Pavlakovic, M.J.S. Lowe, P. Cawley, High-frequency low-loss ultrasonic modes in imbedded bars, *ASME Journal of Applied Mechanics* 68 (2001) 67–75.
[26] G.A. Washer, R.E. Green Jr., R.B. Pond Jr., Velocity constants for ultrasonic stress measurement in prestressing tendons, *Research in Nondestructive Evaluation* 14 (2002) 81–94.
[27] M.D. Beard, M.J.S. Lowe, P. Cawley, Ultrasonic guided waves for inspection of grouted tendons and bolts, *ASCE Journal of Materials in Civil Engineering* 15 (2003) 212–218.
[28] F. Lanza di Scalea, P. Rizzo, F. Seible, Stress measurement and defect detection in steel strands by guided stress waves, *ASCE Journal of Materials in Civil Engineering* 15 (2003) 219–227.